Journal of Power Sources 196 (2011) 9830–9834

Contents lists available at ScienceDirect

Journal of Power Sources

journal homepage: www.elsevier.com/locate/jpowsour

Short communication

In situ lithiation of TiS_2 enabled by spontaneous decomposition of Li_3N

Tom A. Yersak, James E. Trevey, Se-Hee Lee*

Department of Mechanical Engineering, University of Colorado at Boulder, Boulder, CO 80309-0427, USA

ARTICLE INFO

Article history:
Received 19 May 2011
Received in revised form 15 July 2011
Accepted 16 July 2011
Available online 22 July 2011

Keywords:
Titanium sulfide
Lithium nitride
Solid-state
In situ
Lithiation

ABSTRACT

We report on a novel method for in situ lithiation of lithium free TiS_2 using Li_3N in an all-solid-state battery configuration. This method was tested using a Li_3N–TiS_2–$80Li_2S{:}20P_2S_5$ composite positive electrode and an indium metal negative electrode. It is shown that approximately 37% of Li_3N spontaneously decomposes during composite preparation regardless of the composition. Solid-state battery cells built with a 3:1 stoichiometric ratio of Li:Ti demonstrated a high 1st cycle charge capacity of 287 mAh g^{-1}, 20% greater than the theoretical capacity of TiS_2 at 239 mAh g^{-1}. The difference provides an excess capacity in the indium metal negative electrode.

1. Introduction

Lithium free layered transition metal dichalcogenides are promising alternatives to high voltage electrode materials like $LiCoO_2$ [1]. While layered dichalcogenides often have a lower operating voltage, they exhibit comparable energy densities to $LiCoO_2$. TiS_2 has a theoretical specific energy density of 550 Wh kg^{-1}, while $LiCoO_2$ yields a theoretical specific energy density of 500 Wh kg^{-1} [2]. There are numerous advantages to using low voltage active materials. Namely, lower voltage materials often have an increased stability with solid state electrolytes (SSE). $LiCoO_2$ suffers from interfacial instability with SSEs in all-solid-state batteries [3,4]. The formation of a solid electrolyte interphase between electrode and SSE particles often results in degraded cell performance [5]. Another degradation phenomenon occurs in a liquid cell configuration as a result of liquid electrolyte reactivity [6]. Various electrode coatings techniques have been employed to suppress interfacial reactions [7–9]. The increased stability of TiS_2 with SSE eliminates the need for such costly material processing. TiS_2 is also safer because it cannot be overcharged. Unlike Li_xCoO_2, which undergoes an irreversible phase transition for $x < 1/2$, Li_xTiS_2 exhibits only one highly reversible phase for $0 < x < 1$ [10].

For these reasons, previous work has explored designing TiS_2 based all-solid-state batteries [11,12]. All-solid-state batteries address many of the safety issues associated with conventional liquid cells; namely, solvent leakage and flammability [13]. Many solid state batteries utilize sulfide based glass electrolytes for their high conductivity and good stability with lithium metal [14]. Regardless, many researchers utilize an indium metal anode for its superior safety [15]. As a result, the construction of a cell with a lithium free positive electrode material is difficult because conventional anode materials like graphite are lithium free. Conventional methods of incorporating lithium ions into cells include electrochemical processes [16], chemical treatment of electrode material with n-butyllithium [17,18], sacrificial lithium electrodes [19], lithium alloys like In–Li or Al–Li [15,20] or by adding stabilized lithium powder to electrode material [21].

This paper proposes a novel method for the in situ lithiation of lithium free electrode materials like TiS_2 using Li_3N in an all-solid-state battery configuration. Li_3N was considered a candidate for use as a highly ionically conductive anisotropic SSE. Indeed, single crystals of Li_3N have exhibited conductivities of 1.2×10^{-3} S cm^{-1} in directions parallel to the Li_2N^- planes of Li_3N's layered structure [22]. Previous work by Knutz and Skaarup investigated the performance of all-solid-state batteries using a Li_3N–TiS_2 composite with limited success [23,24]. Li_3N's low thermodynamic decomposition potential, $\Delta G^\circ/3F = 0.44$ V [25], limited its use as a practical SSE. While the low decomposition voltage of Li_3N makes for a poor SSE, it does make Li_3N a perfect candidate for in situ lithiation. Using the Nernst equation, Li_3N's decomposition potential, and an average potential of 2.1 V for TiS_2 versus lithium, it can be shown that Li_3N will spontaneously decompose when mixed with TiS_2:

$$TiS_{2(s)} + 0.33Li3N_{(s)} \leftrightarrow LiTiS_{2(s)} + 0.167N_{2(g)};$$
$$\Delta G^\circ = -160\ \text{kJ mol}^{-1} \quad (1)$$

* Corresponding author. Tel.: +1 303 492 7889; fax: +1 303 492 3498.
E-mail address: sehee.lee.@colorado.edu (S.-H. Lee).

0378-7753/$ – see front matter © 2011 Elsevier B.V. All rights reserved.
doi:10.1016/j.jpowsour.2011.07.059

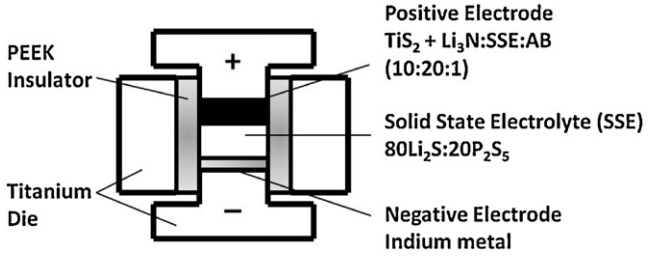

Fig. 1. Schematic diagram titanium/PEEK test die cross-section for all-solid-state battery.

Indeed, a previous study has demonstrated that Li_3N decomposes merely by grinding TiS_2 and Li_3N together [26]. It will be shown that the addition of Li_3N to composite electrodes can precisely lithiate TiS_2 upon cycling and provide excess capacity in the anode to account for irreversible capacity loss.

2. Materials and methods

The preparation of $80Li_2S{:}20P_2S_5$ (mol%) SSE followed a previously reported planetary ball milling process [14] with the exclusion of solid electrolyte pelletization prior to heat treatment. Reagent grade powders of Li_2S (Alfa-Aesar, 99.9%) and P_2S_5 (Sigma–Aldrich, 99%) were used as starting materials. Composite electrodes were prepared by mixing TiS_2 (Sigma–Aldrich, 99.9%), Li_3N (Alfa-Aesar, 99.4%), SSE $80Li_2S{:}20P_2S_5$ (mol%), and acetylene black (AB) (Sigma–Aldrich, 50% compressed) at a weight ratio of $10-x{:}x{:}20{:}1$, respectively in an agate mortar and pestle. Progressively larger amounts of Li_3N were added to the composite electrode with $x = 0.93$, 1.3, 1.7, and 2.4 corresponding to the stoichiometric Li:Ti ratios of 1:1, 1.5:1, 2:1 and 3:1, respectively. The stoichiometric Li:Ti ratio relates the amount of TiS_2 to the amount lithium provided by Li_3N decomposition. Therefore, assuming complete decomposition of Li_3N, the 1:1 ratio would represent $y = 1$ for Li_yTiS_2.

The construction of solid state test cells utilizes a polyaryletheretherketone (PEEK) mold ($\varphi = 1.3$ cm) with two titanium plungers for current collectors and a titanium outer shell [27]. Fig. 1 provides a schematic of the test cell setup used in this study. 150 mg of SSE powder is cold pressed at 1 metric ton for 1 min. 10 mg of composite electrode and the pre-pressed SSE are cold pressed together at 5 metric tons for 5 min. Indium foil (Alfa-Aesar, $t = 0.75$ mm) is attached to the SSE surface by pressing at 0.5 metric tons momentarily. All galvanostatic charge–discharge cycling was performed in a dry argon environment at room temperature using an Arbin BT2000. The first cycle was carried out with cut off voltages of 0.9 and 2.4 V and a current density of 44 $\mu A\,cm^{-1}$ ($C/10$). The current density was increased to 88 $\mu A\,cm^{-1}$ ($C/5$) for all subsequent cycles.

Materials were characterized by XRD measurement with Cu-Kα radiation. Cycled composite electrode material was obtained by constructing cells with 100 mg of the 3:1 stoichiometric Li:Ti ratio composite electrode. Upon completion of the 11th discharge and 1st charge cycle, the cells were disassembled and the composite electrode material recovered. 50 mg of material was ground in mortar and pestle and sealed under argon in an airtight aluminum holder with beryllium windows before being mounted on the X-ray diffractometer (PANalytical, PW3830).

3. Results and discussion

XRD analysis is used to reveal the extent of TiS_2 lithiation by Li_3N decomposition. Fig. 2 presents the XRD spectra for individual composite electrode components prior to mixing and the XRD spectra

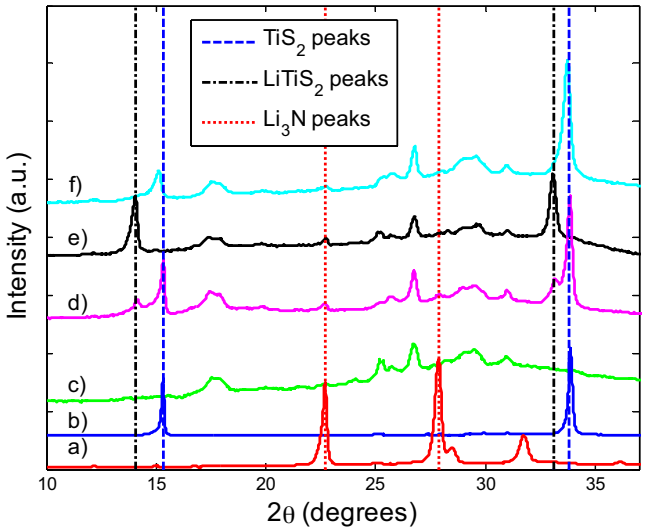

Fig. 2. XRD measurement of (a) Li_3N, (b) TiS_2, (c) $80Li_2S{-}20P_2S_5$ SSE, (d) uncycled composite electrode, (e) composite electrode after 11th discharge and (f) composite electrode after 1st charge.

for ex situ composite electrode materials. Individual composite electrode components studied are Li_3N, TiS_2, and $80Li_2S{-}20P_2S_5$ SSE. Ex situ composite electrode material (3:1 stoichiometric Li:Ti ratio) was recovered and studied before galvanostatic cycling (uncycled), after the 11th discharge and after the 1st charge. Charging corresponds to the de-lithiation of $LiTiS_2$ while discharging corresponds to the lithiation of TiS_2. Peaks from the beryllium windows appear at approximately 25°. Vertical dotted lines highlight the important diffraction peaks for the materials of interest.

TiS_2 shows two predominant peaks at 15.25° and 33.86° and are indicated by the blue dotted lines in Fig. 2. These two peaks are evident in the XRD spectrum for the uncycled composite electrode. It is concluded that despite manual grinding, a large amount of TiS_2 still remains in the uncycled composite electrode. However, the broadening of these peaks indicates partial lithiation of some TiS_2 in the composite electrode material. Two additional peaks are observed at the smaller angles of 14.07° and 33.15° and are indicated by the black dotted lines in Fig. 2. According to Bragg's law of diffraction, an increase in lattice d-spacing is associated with a decrease in the angle of diffraction. Upon intercalation, it is expected that the insertion of lithium ions will expand the lattice in certain crystallographic directions. Indeed, the two new peaks closely correspond to previously reported very strong peaks of the 1 T polytype of $LiTiS_2$ at 14.34° and 33.22° [28]. From the presence of these new peaks at smaller angles, it is determined that Li_3N decomposition proceeds to fully lithiate some TiS_2 to $LiTiS_2$ just by the manual grinding of powders. This result agrees with previous work demonstrating Li_3N's reactivity with TiS_2 upon mixing [26].

By the completion of the 11th discharge, TiS_2 is fully lithiated to $LiTiS_2$. It is observed that the predominant TiS_2 peaks completely shift from 15.25° and 33.86° to 14.07° and 33.15°, respectively. The repeated electrochemical cycling of the composite electrode material facilitates Li_3N decomposition and the complete lithiation of TiS_2 to $LiTiS_2$. After the first charge, peaks for TiS_2 are observed at 15.11and 33.73. Although these peaks are slightly shifted from pristine TiS_2 peaks at 15.25° and 33.86°, this result demonstrates that TiS_2 does not undergo significant structural changes and that the intercalation reaction in the presence of Li_3N remains largely reversible.

Li_3N is not completely decomposed upon composite grinding or even upon cycling. Li_3N peaks at 22.7° and 27.8° are observed

Table 1
Percentage Li_3N decomposed upon first charge for composite electrodes of varying Li:Ti stoichiometric ratios.

Li:Ti stoich. ratio	TiS_2 (mg)	Li_3N (mg)	1st charge capacity (mAh g^{-1})	Reacted Li_3N (mg)	Reacted L_3N (%)
1:1	2.93	0.30	88	0.11	37.08
1.5:1	2.79	0.43	135	0.16	37.79
2:1	2.67	0.55	191	0.20	35.81
3:1	2.46	0.77	287	0.30	39.56

for all composite electrode materials before and after cycling. The red set of dotted lines in Fig. 2 track the two most predominant Li_3N peaks. Assuming a complete Faradaic process, we can calculate the percentage of Li_3N decomposed upon the first charge. Table 1 shows the percentage of Li_3N decomposed remains relatively constant at approximately 37% regardless of the changing electrode composition. Additional peaks observed in the composite electrode materials are consistent with those peaks observed for SSE. Based on this observation, the XRD measurements indicate no obvious presence of nitrogen based decomposition products.

SEM micrographs of composite electrode components are shown in Fig. 3. TiS_2 particles have an average diameter of 5–10 μm, SSE particles an average diameter of 10 μm and Li_3N particles an average diameter of 1–5 μm. With these relative particle sizes, it is reasonable that some smaller Li_3N particles are isolated from TiS_2 by the bulk of SSE particles in the composite electrode. Fig. 3d depicts the stoichiometric 3:1 Li:Ti ratio electrode composite. It is observed that the plate-like-particles of TiS_2 are isolated from some of the smaller Li_3N particles by the presence of larger SSE particles. It was observed that a constant 37 wt% of Li_3N was decomposed regardless of composite composition. It is important to note that adding additional Li_3N to the larger stoichiometric Li:Ti ratio composites is done so at the expense of TiS_2. In large ratio composites, more Li_3N may be isolated from TiS_2 by the larger ratio of SSE with respect of TiS_2 present in the composite.

Fig. 4a presents the 1st cycle voltage profiles for composite electrodes corresponding to the results presented in Table 1. The cells are charged first, corresponding to the de-lithiation of $LiTiS_2$. If Li_3N did not successfully decompose to lithiate TiS_2, the cells would show no capacity upon initial charging. As expected, cells with a larger Li:Ti ratio show a higher degree of lithiation. The cell built with a 3:1 Li:Ti ratio composite demonstrated a 1st cycle charge capacity of 287 mAh g^{-1}; 48 mAh g^{-1} greater than the theoretical capacity of TiS_2 of 239 mAh g^{-1}. From the XRD study, it is known that some TiS_2 is lithiated to within Li_xTiS_2 ($0 > x \geq 1$) just by preparing the composite. However, the uncycled composite electrode XRD spectrum still exhibited the dominant TiS_2 peaks indicating incomplete lithiation by composite grinding. As the observed 1st cycle charge capacity cannot be supplied entirely by the reversible lithium de-lithiation of $LiTiS_2$, the excess capacity is observed as irreversible decomposition of Li_3N upon cycling. The excess capacity is not a result of electrolyte decomposition as the SSE diffraction peaks remain unchanged after cycling. This indicates no SSE structural changes and therefore it is unlikely that the SSE reacts with Li_3N. Such a high initial charge capacity will leave excess lithium in the indium negative electrode upon completion of the first discharge. Similar to the excess capacity provided by the stabilized lithium powder lithiation method [21], the excess capacity provided by Li_3N can be used to offset irreversible capacity loss of the cell. For cells with stoichiometric Li:Ti ratios less than 3:1, the

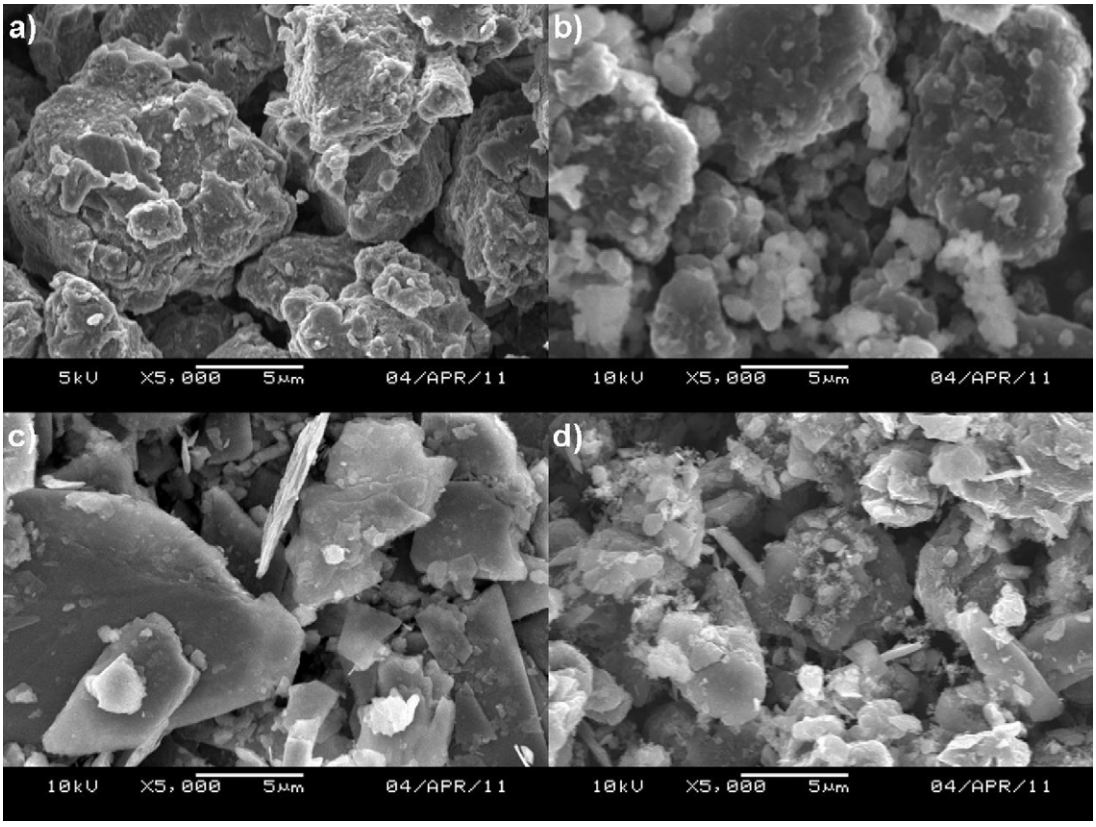

Fig. 3. SEM micrographs of (a) SSE $80Li_2S{:}20P_2S_5$, (b) Li_3N, (c) TiS_3 and (d) hand-mixed 3:1 Li:Ti stoichiometric ratio composite electrode.

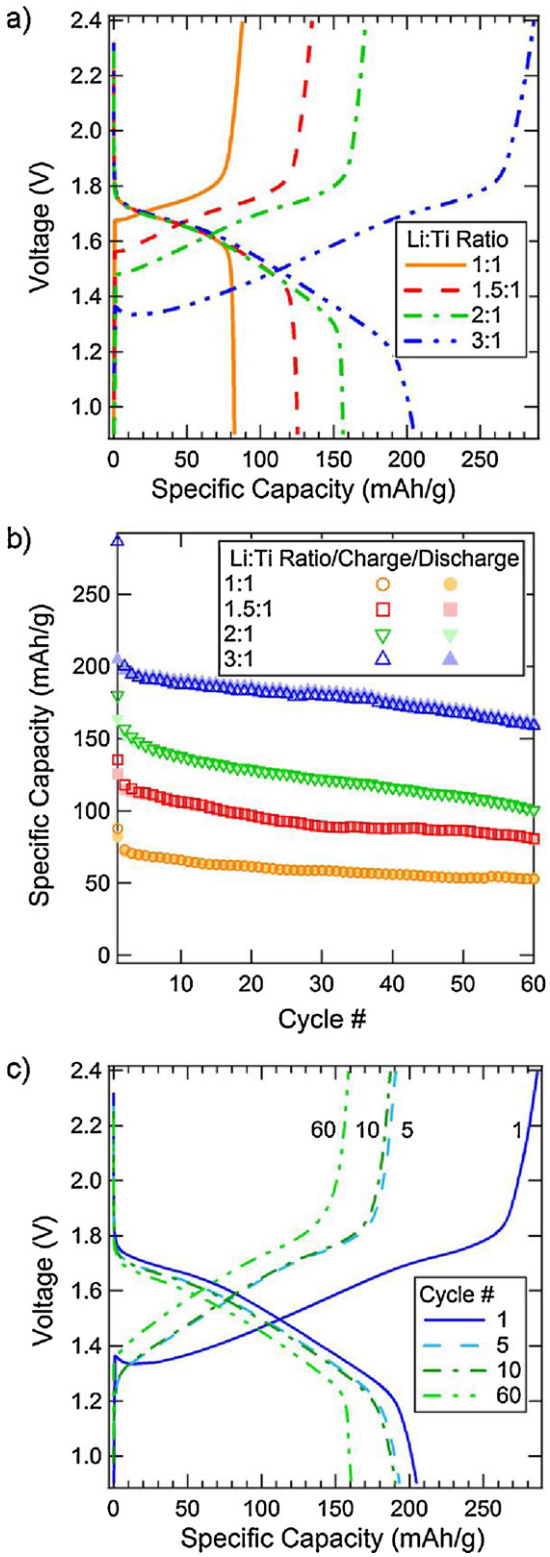

Fig. 4. (a) 1st cycle charge/discharge voltage profiles and (b) cycle performance of cells with Li_3N–TiS_2 composite electrodes with varying Li:Ti stoichiometric ratios. (c) Charge/discharge voltage profiles for 3:1 stoichiometric Ti:Li ratio composite electrode cell, Li_3N–TiS_2–SSE composite/SSE/In.

decomposition of Li_3N was insufficient to fully lithiate TiS_2. A significant drop in 1st cycle charge and discharge capacity is observed when Li_3N–TiS_2 composite electrodes were prepared without AB. Normally, TiS_2 has such good electronic conductivity that AB is not required [29]. The need for conductive additive may be due $N_{2(g)}$, formed by the in situ decomposition of Li_3N, expanding the electrode and breaking particle contact. The addition of AB may help maintain electrical contact of TiS_2 particles.

Cells built with Li_3N–TiS_2 composite electrodes exhibit good cycling performance. Fig. 4b presents the charge cycling performance for electrodes with varying Li:Ti stoichiometric ratios. The observed initial capacity drop is a result of Li_3N decomposition predominantly occurring during the first cycle. The voltage profiles for the 1st, 5th, 20th and 60th cycles of the cell built with a 3:1 stoichiometric Li:Ti ratio composite are presented in Fig. 4c. Upon the 60th cycle, the 3:1 composite cell maintains 78% of its 1st discharge capacity. Unlike the excess charge capacity of 1st cycle, we see little difference between the charge and discharge capacities for the 5th, 20th and 60th cycles.

The previously mentioned work by Knutz and Skaarup [24] explored cells made with a TiS_2–Li_3N composite electrode. A steady loss in cell capacity was reversed by decreasing the *C*-rate. The authors attributed the poor cycling performance not to irreversible capacity loss, but to a decrease in Li^+ transport kinetics. This study has shown that Li_3N decomposes in the presence of TiS_2 upon cycling. As Li_3N particles decompose, ionic conduction pathways are broken. The effect of fewer conduction pathways would be offset by cycling the cell at slower rates and allowing diffusion processes time to progress. As shown in our study, the decomposition of Li_3N would eliminate conduction pathways in a TiS_2–Li_3N composite electrode. The Li_3N–TiS_2–SSE composite electrodes in this study are constructed predominantly with $80Li_2S{:}20P_2S_5$ SSE. Such a large amount of $80Li_2S{:}20P_2S_5$ SSE should provide a stable network of Li^+ conduction pathways. However, it is important to remember that only 37% of the Li_3N decomposes upon the 1st cycle and each cell still loses approximately 20% of its 1st cycle discharge capacity by the 60th cycle. It is concluded that the excess Li_3N remaining in the composite electrode after the initial charge may not be entirely isolated from TiS_2 by SSE particles. Observed capacity degradation may be a result of Li_3N slowly degrading, breaking ionic conduction pathways and therefore isolating TiS_2 particles. Current work is examining the use of a mechanochemical milling process to lithiate TiS_2 ex situ and eliminates the presence of excess Li_3N in the composite electrode.

4. Conclusions

Li_3N to lithiate TiS_2 in situ. The method of Li_3N in situ lithiation requires no special fabrication techniques or highly explosive chemicals. Li_3N can be added to the composite material until the desired degree of lithiation is achieved. A 3:1 stoichiometric Li:Ti composite electrode demonstrated a 287 mAh g^{-1} 1st charge capacity, or 48 mAh g^{-1} greater than TiS_2's theoretical capacity. It is shown that an excess of Li_3N can be added to account for irreversible capacity loss. Li_3N–TiS_2 composite electrodes also show good cycling performance with the 3:1 Li:Ti stoichiometric ratio electrode maintaining 78% of its 1st cycle discharge capacity upon the 60th cycle. Li_3N in situ lithiation opens up the possibility of safely utilizing many lithium free electrode materials in all-solid-state batteries.

Acknowledgements

Funding provided by NSFGRFP and DARPA grant # FA8650-08-1-7839. Funding sources had no involvement in the decision making of this study.

References

[1] M.S. Whittingham, Progress in Solid State Chemistry 12 (1978) 41–99.

[2] T.B. Reddy, S. Hossain, in: D. Linden, T.B. Reddy (Eds.), Handbook of Batteries, McGraw-Hill, New York, 2002.
[3] A. Sakuda, A. Hayashi, M. Tatsumisago, Chemistry of Materials 22 (2010) 949–956.
[4] A. Brazier, L. Dupont, L. Dantras-Laffont, N. Kuwata, J. Kawamura, J.M. Tarascon, Chemistry of Materials 20 (2008) 2352–2359.
[5] J.E. Trevey, Y.S. Jung, S.-H. Lee, Journal of Power Sources 195 (2010) 4984–4989.
[6] L.A. Riley, S. Van Atta, A.S. Cavanagh, Y. Yan, S.M. George, P. Liu, A.C. Dillon, S.-H. Lee, Journal of Power Sources 196 (2011) 3317–3324.
[7] A. Sakuda, H. Kitaura, A. Hayashi, K. Tadanaga, M. Tatsumisago, Journal of Power Sources 189 (2009) 527–530.
[8] H. Kitaura, A. Hayashi, K. Tadanaga, M. Tatsumisago, Solid State Ionics 192 (2011) 304–307.
[9] K.H. Choi, J.H. Jeon, H.K. Park, S.M. Lee, Journal of Power Sources 195 (2010) 8317–8321.
[10] M.S. Whittingham, Journal of the Electrochemical Society 123 (1976) 315–320.
[11] J.R. Akridge, H. Vourlis, Solid State Ionics 28–30 (1988) 841–846.
[12] K. Iwamoto, N. Aotani, K. Takada, S. Kondo, Solid State Ionics 70–71 (1994) 658–661.
[13] F. Mizuno, A. Hayashi, K. Tadanaga, M. Tatsumisago, Advanced Materials 17 (2005) 918–921.
[14] A. Hayashi, S. Hama, F. Mizuno, K. Tadanaga, T. Minami, M. Tatsumisago, Solid State Ionics 175 (2004) 683–686.
[15] K. Takada, N. Aotani, K. Iwamoto, S. Kondo, Solid State Ionics 86–88 (1996) 877–882.
[16] C.-K. Huang, S. Surampudi, A.I. Attia, G. Halpert, US Patent # 5,436,093 (1995).
[17] M.B. Dines, Materials Research Bulletin 10 (1975) 287–291.
[18] M.S. Whittingham, M.B. Dines, Journal of the Electrochemical Society 124 (1977) 1387–1388.
[19] T. Sasaki, T. Sakai, K. Tahara, US Patent # 5,556,721 (1996).
[20] B.M.L. Rao, R.W. Francis, H.A. Christopher, Journal of the Electrochemical Society 124 (1977) 1490–1492.
[21] C.R. Jarvis, M.J. Lain, Y. Gao, M. Yakovleva, Journal of Power Sources 146 (2005) 331–334.
[22] U.v. Alpen, A. Rabenau, G.H. Talat, Applied Physics Letters 30 (1977) 621–623.
[23] B. Knutz, S. Skaarup, Solid State Ionics 9–10 (1983) 371–374.
[24] B. Knutz, S. Skaarup, Solid State Ionics 18–19 (1986) 783–787.
[25] A. Rabenau, Solid State Ionics 6 (1982) 277–293.
[26] J.R. Rea, D.L. Foster, P.R. Mallory, Materials Research Bulletin 14 (1979) 841–846.
[27] J. Trevey, J.S. Jang, Y.S. Jung, C.R. Stoldt, S.-H. Lee, Electrochemistry Communications 11 (2009) 1830–1833.
[28] K.M. Colbow, J.R. Dahn, R.R. Haering, Journal of Power Sources 26 (1989) 301–307.
[29] A.H. Thompson, Physical Review Letters 35 (1975) 1786.